Gold nanostars as thermoplasmonic nanoparticles for optical heating

R. Rodríguez-Oliveros* **and José A. Sánchez-Gil**

Instituto de Estructura de la Materia, Consejo Superior de Investigaciones Científicas, Serrano 121, 28006 Madrid, Spain

*Rogelio@iem.cfmac.csic.es

Abstract: Gold nanostars are theoretically studied as efficient thermal heaters at their corresponding localized surface-plasmon resonances (LSPRs). Numerical calculations are performed through the 3D Green's Theorem method to obtain the absorption and scattering cross sections for Au nanoparticles with star-like shape of varying symmetry and tip number. Their unique thermoplasmonic properties, with regard to their (red-shifted) LSPR wavelentgh, ($\sim$ 30-fold increase) steady-state temperature, and scattering/absorption cross section ratios, make them specially suitable for optical heating and in turn for cancer thermal therapy.

OCIS codes: (240.6680) Surface plasmons; (250.5403) Plasmonics; (170.5180) Photodynamic therapy.

References and links

1. N. J. Halas, S. Lal, C. Wei-Shun, S. Link, and P. Nordlander, "Plasmons in strongly coupled metallic nanostructures," Chem. Rev. **111**, 3913–3961 (2011).
2. A. G. Skirtach, C. Dejugnat, D. Braun, A. S. Susha, A. L. Rogach, W. J. Parak, H. Möhwald, and G. B. Sukhorukov, "The role of metal nanoparticles in remote release of encapsulated material," Nano Lett. **5**, 1371–1377 (2005).
3. M. A. Barral and A. M. Llois, "Photothermal imaging of nanometer-sized metal particles among scatterers," Science **297**, 1160–1163 (2002).
4. C. Loo, A. Lowery, N. J. Halas, J. L. West, and R. Drezek, "Immunotargeted nanoshells for integrated cancer imaging and therapy," Nano Lett. **5**, 709–711 (2005).
5. C. Loo, A. Lin, L. Hirsch, M. H. Lee, J. Barton, N. J. Halas, and J. L. West, "Nanoshell-enabled photonics-based imaging and therapy of cancer," Technol. Cancer Res. Treat. **3**, 33–40 (2004).
6. A. M. Gobin, M. H. Lee, N. J. Halas, W. D. James, R. A. Drezek, and J. L. West, "Near-infrared resonant nanoshells for combined optical imaging and photothermal cancer therapy," Nano Lett. **7**, 1929–1934 (2007).
7. A. O. Govorov and H. H. Richardson, "Generating heat with metal nanoparticles we describe recent studies on photothermal effects using colloidal," Nano Today **2**, 30–38 (2007).
8. F. X. Gu, R. Karnik, A. Z. Wang, F. Alexis, E. Levy-Nissenbaum, S. Hong, R. S. Langer, and O. C. Farokhzad, "Targeted nanoparticles Over the past decade , there has been an increasing interest in using fabrication of targeted NPs using microfluidic devices," Nano Today **2**, 14–21 (2007).
9. P. K. Jain, I. H. El-Hayed, and M. A. El-sayed, "Au nanoparticles target cancer," Nano Today **7**, 1929–1934 (2007).
10. W. Zhao and J. M. Karp, "Tumour targeting: Nanoantennas heat up," Nature Mater. **8**, 453–454 (2009).
11. V. Giannini, R. Rodríguez-Oliveros, and J. A. Sánchez-Gil, "Surface plasmon resonances of metallic nanostars/nanoflowers for surface-enhanced Raman scattering," Plasmonics **5**, 99–104 (2010).
12. A. Tassadit, D. Macías, J. A. Sanchez-Gil, and R. Rodríguez-Oliveros, "Metal nanostars: Stochastic optimization of resonant scattering properties," Superlattices Microst. **49**, 288–293 (2011).
13. P. Senthil Kumar, I. Pastoriza-Santos, B. Rodríguez-González, F. J. García de Abajo, and L. M. Liz-Marzán, "High-yield synthesis and optical response of gold nanostars," Nanotechnology **19**, 015606 (2008).
14. C. Hrelescu, T. K. Sau, A. L. Rogach, F. Jäckel, G. Laurent, L. Douillard, and F. Charra, "Selective excitation of individual plasmonics hotspots at the tips of single gold nanostars," Nano Lett. **11**, 402–407 (2011).

#155373 - $15.00 USD Received 27 Sep 2011; revised 2 Dec 2011; accepted 6 Dec 2011; published 23 Dec 2011

15. S. Mazzuco, O. Stéphan, C. Colliex, I. Pastoriza-Santos, L. M. Liz-Marzán, and F. J. García de Abajo, "Spatially resolved measurements of plasmonic eigenstates in conplex-shaped, asymmetric nanoparticles: gols nanostars," Eur. Phys. J. Appl. Phys. **54**, 33512 (2011).
16. G. Baffou, P. M. Kreuzer, F. Kulzer, and R. Quidant, "Temperature mapping near plasmonic nanostructures using fluorescence polarization anisotropy," Opt. Express **17**, 3291–3298 (2009).
17. B. Van de Broek, D. Grandjean, J. Trekker, J. Ye, K. Verstreken, G. Maes, G. Borghs, S. Nikitenko, L. Lagae, C. Bartic, K. Temst, and M. J. Van Bael, "Temperature determination of resonantly excited plasmonic branched gold nanoparticles by X-ray absorption spectroscopy," Small **7**, 2498–2506 (2011).
18. M. Honda, Y. Saito, N. I. Smith, K. Fujita, and S. Kawata, "Nanoscale heating of laser irradiated sigle gold nanoparticles in liquid," Opt. Express **19**, 12375–12383 (2011).
19. R. Rodríguez-Oliveros and J. A. Sanchez-Gil, "Localized surface-plasmon resonances on single and coupled nanoparticles through surface integral equations for flexible surface," Opt. Express **19**, 12208–12219 (2011).
20. J. Gielis, "A generic geometric transformation that unifies a wide range of natural and abstract shapes." Am. J. Bot. **90**, 333–338 (2003).
21. P. B. Johnson and R. W. Christy, "Optical constants of the noble metals," Phys. Rev. B **6**, 4370–4379 (1972).
22. G. Baffou, R. Quidant, and C. Girard, "Heat generation in plasmonic nanostructures: Influence of morphology," Appl. Phys. Lett. **94**, 153109 (2009).
23. G. Baffou, R. Quidant, and C. Girard, "Thermoplasmonics modeling: A Greens function approach," Phys. Rev. B **82**, 1–11 (2010).
24. G. Baffou, R. Quidant, and F. J. García de Abajo, "Nanoscale control of optical heating in complex plasmonic systems," ACS Nano **4**, 709–716 (2010).
25. J. Xie, Q. Zhang, J. Y. Lee, and D. I. C. Wang, "The synthesis of SERS-Active gold nanoflower tags for in vivo applications," ACS Nano **2**, 2473–2480 (2008).
26. T. Vo-dinh, A. Dhawan, S. J. Norton, C. G. Khoury, H. Neng Wang, V. Misra, and M. D. Gerhold, "Plasmonic nanoparticles and nanowires: design, fabrication and application in sensing," J. Phys. Chem. C pp. 7480–7488 (2010).
27. E. Nalbant Esenturk and A. R. Hight Walker, "Surface-enhanced Raman scattering spectroscopy via gold nanostars," J. Raman Spectrosc. **40**, 86–91 (2009).
28. J. M. Cabrera-Trujillo, J. M. Montejano-Carrizales, J. L. Rodríguez-López, W. Zhang, J. J. Velázquez-Salazar, and M. José-Yacaman, "Controlling and growth of stellated gold clusters: experimental synthesis and theoretical study," J. Phys. Chem. C **114**, 21051–21060 (2010).

1. Introduction

In recent years, it has been found that metallic nanoparticles (NPs), apart from their intense use for enhanced-spectroscopy applications [1], also exhibit a great potential in optical heating applications such as drug delivery [2], imaging [3–5], and photothermal cancer therapy [6–10]. Heating metallic nanoparticles, previously allocated into cancerous cells, with an impinging laser beam, results in the stop of the cellular activity, thus leading to either shrinking the tumour size, or slowing down its spread. Obviously, the larger the NPs temperature, the more effectively the cell activity is stopped. That is the reason why most of the effort in this novel field is focused on exploiting the huge electromagnetic fields produced on the nanoparticles through localized surface plasmon resonances (LSPR). Indeed, it has been shown that Au NPs can be heated up to temperatures five orders of magnitude larger than those reached with dyes originally used in early demonstrations of photothermal tumour therapy [9]. This fact leads to a reduction of the irradiation energy, considerably shrinking the probability of damaging non-cancerous cells.

Along with these promising experimental results, on the other hand, it has been recently shown that metallic nanostars (NSs) notably enhance local electromagnetic fields at LSPRs, making them good candidates for surface-enhanced Raman spectroscopy (SERS) substrates without any induced aggregation [11–15]. Additionally recent thermometric measurements of metallic NPs [16–18] have shown the need of deep theoretical studies of the thermal properties of metallic NPs. In this Letter, we show that metallic nanostars are not only suitable for sensing application, but can also play the role of heat sources considerably more efficient than the commonly studied nanospheres, as a result of the large absorption cross section at the LSPR. Making use of the 3D Green's Theorem (surface integral equations) method (3DGTm) for flexible-shape NPs that we have recently introduced [19], we calculate rigorously the local

#155373 - $15.00 USD Received 27 Sep 2011; revised 2 Dec 2011; accepted 6 Dec 2011; published 23 Dec 2011

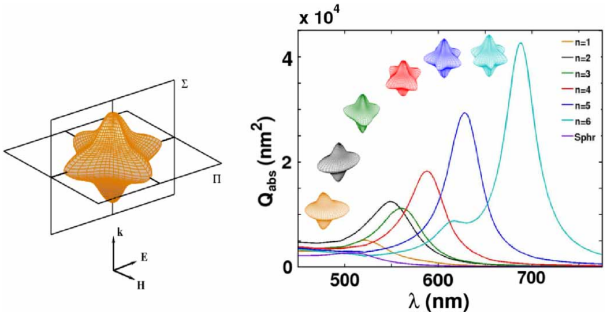

Fig. 1. (a) Schematic representation of a 4-fold nanostar, with two relevant symmetry planes: the plane Π where the number of tips is varied and the polarization plane Σ. (b) Absorption cross sections for Au nanostars with different number of tips from S_1 to S_6, along with that for the equivalent Au nanosphere.

electromagnetic field distribution on the surface of the nanostars at the LSPRs, from which the absorption cross section is worked out, as needed to determine the steady-state temperature of a metallic NP.

2. LSPRs of gold nanostars

Let us consider a NS whose geometrical shape is described as a deformable parametric surface called *Supershape* [20], which depends on certain parameters that basically modify the sphere formula in spherical coordinates. Particularly, we fix a configuration of parameters that allow us to change the number of tips in a star-like volume, preserving its shape. In order not to introduce too much complexity in the system under study, we only vary the number of tips in the plane Π (see Fig. 1(a)) from $n = 1$ to $n = 6$. In the perpendicular plane Σ, the symmetry of the number of star tips is kept constant in such a way that two opposing tips, one pointing upwards and the other one downwards. We will refer to the nanostar with n tips in the plane Π as S_n. Such star-like shapes indeed closely resemble those of fabricated colloidal NSs [13].

In Fig. 1(b) the absorption cross section is plotted for NSs made of gold described by the dielectric constant reported in reference [21]. The incident field is a plane wave impinging from the bottom, its plane of incidence being the plane Σ, Fig. 1(a). NSs have arms 40 nm long, and increasing number of tips. The LSPRs for Au-NSs are red-shifted when the number of tips in the plane Π increases from S_1 to S_6: λ_{LSP} (nm)=521, 548, 560, 587, 628, 688, respectively. In Fig. 2(a-f) we have plotted the norm of the surface electric field (SF) of the NSs in logarithmic scale. As a general result, the SF is accumulated on the vertex of the NSs, thereby providing large field enhancements, about $|E|^2 \sim 10^4$. Incidentally, these values make nanostars suitable for SERS applications [11, 13]. Essentially, such SF patterns results from the dipolar character on the plane Π of the corresponding lowest-energy LSPR. In addition, SF enhancements at the LSPR grow for increasing number of tips from S_1 to S_6, in agreement also with the absorption cross section in Fig. 1(b), that shows the same trend from S_1 to S_6; except for S_2, which has an absorption cross section and SF slightly larger than expected, presumably due to its 2-tip symmetry along the polarization axis, specially suited to match the dipolar LSPR pattern. In this regard, the NS asymmetry on the plane Σ along the polarization axis reduces its quality as dipole-like resonant cavity.

3. Temperature profile of optically heated gold nanostars

From the point of view of the applicability for thermal therapy, such large absorption cross sections make Au NSs good candidates to be used as heat sources.

#155373 - $15.00 USD Received 27 Sep 2011; revised 2 Dec 2011; accepted 6 Dec 2011; published 23 Dec 2011

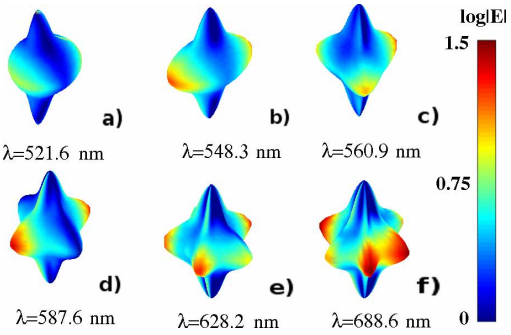

Fig. 2. Distribution of electric field amplitudes in logarithmic scale on the surface of the Au nanostars at their corresponding LSPR wavelengths for an incident electric field contained into the plane Σ (see Fig. 1(a)).

In fact, in recent works [22–24], G. Baffou and co-workers have developed a useful and simple expression that relates the absorption cross section σ_{abs} with the steady-state temperature T of a NP under the effect of a laser beam, namely:

$$T = \frac{\sigma_{abs} I}{4\pi\kappa r_{\text{eff}}}, \tag{1}$$

where I is the irradiance of the incoming beam and κ is the thermal conductivity of the nanoparticle material or the surrounding medium. r_{eff} is a characteristic geometrical parameter of the NP shape, that is defined as:

$$r_{\text{eff}} = \sum_i \sum_j (A^{-1})_{ij}, \tag{2}$$

where A_{ij} is the matrix,

$$A_{ij} = \frac{1}{|r_i - r_j|}, \tag{3}$$

r_i, r_j, being position vectors of the points inside the NP. Equation 1 is the expression for the equilibrium temperature of a homogeneous sphere made of a material characterized by κ, where r_{eff} correspond to the radius of the sphere. For non-spherical NPs, the main contribution to the effective radius comes from the furthest points on the surface. The *supershape* allows us to chose its parameters in such a way that r_{eff} is almost constant with the number of tips of the NSs, $r_{\text{eff}} \approx 26$ nm (see Table 1).

From equations 1 and 2, it is clear that the steady-state temperature of two metallic NPs with the same $r_{\text{eff}} = r = r'$, and different frequencies $\tilde{\omega}$, ω follow:

$$\tau_E(\tilde{\omega}, \omega) = \frac{T'}{T} = \frac{\sigma'_{abs}(\tilde{\omega})}{\sigma_{abs}(\omega)}. \tag{4}$$

Thus the temperature relative factor τ_E depends in this case only on the absorption cross section ratio. Since r_{eff} for the NSs considered here is almost constant, the variation of τ_E with respect to the number of tips will be dominated by the relative height of the absorption cross section at a specific wavelength. Table 1 shows the relative temperature for all the NSs under study, compared to that of nanospheres with the same r_{eff} at the corresponding LSPR wavelength. Note that Au NSs yield temperature larger than the corresponding Au nanosphere, S_6 reaching a 16-fold increase.

In Fig. 3(a) we study the dependence of Q_{abs} and Q_{sca} on the tip sharpness for the Au NS S_4. In order to isolate the effect of the change of the sharpness in the optical response of the

#155373 - $15.00 USD Received 27 Sep 2011; revised 2 Dec 2011; accepted 6 Dec 2011; published 23 Dec 2011

Table 1. LSPR wavelengths λ_p and relative temperature factors τ_E for Au-NSs with given geometrical parameters: n, number of tips in the plane Π; s, the parameter that controls NS tip sharpness; and r_{eff}, effective radius.

n	s	r_{eff}	λ_p	τ_E
1	0.2	25.8	521.6	1.9
2	0.2	26.1	548.3	4.7
3	0.2	26.35	560.9	4.2
4	0.2	26.30	587.6	6.8
5	0.2	26.35	628.2	11
6	0.2	26.8	688.6	16
4	0.3	25.75	525.3	1.75
4	0.175	26.89	650.1	13.6
4	0.125	27.97	860.2	32.

NSs, their volume is kept constant, and equal to the volume of the effective sphere. Two main effects are addressed: i) LSPR shifts to the red for increasing sharpness; ii) The value of Q_{abs} at the LSPR becomes larger. Interestingly, the imaginary part of the dielectric constant of gold, $Im(\varepsilon_{Au})$, has a minimum in the near IR at a wavelength (700nm) slightly larger than the onset of interband transitions, beyond which $Im(\varepsilon_{Au})$ monotonically increases following a Drude metal behavior. Accordingly, a reduction of Q_{abs} in the range of wavelengths ($\lambda \gtrsim 600$ nm) relevant to medical applications might be expected. Q_{abs} of the equivalent sphere is plotted in order to illustrate this fact. The LSPR wavelength of the sphere is $\lambda = 510$ nm; for larger wavelengths the imaginary part of the dielectric constant decreases leading to a decrease of Q_{abs} as well. On the contrary, Q_{abs} of the NSs increases when the LSPR is shifted to the red, even if the imaginary part of the dielectric constant decreases. However, the ratio Q_{abs}/Q_{sca} at the LSPR decreases as expected. In Table (1) we show the values of τ_E at the LSPR for varying tip sharpness in the case of S_4 NS [19]. It clearly reveals that, the sharper the NS tips are, the larger the absorption cross section is at the LSPR. Moreover, the temperature relative factor for the sharper S_4 is about thirty times larger than τ_E for the effective sphere. Thus, sharp Au NSs provide a huge heating efficiency compared to that of the effective Au nanosphere. In Fig. 3(b) the temperature distribution on the plane Π is shown for the sharper Au-NS (S_4 with $s = 0.125$ in Fig. 3(a). The temperature distribution clearly follows the NS shape, the effective heating range being almost restricted to the touching regime. Thus, cells will only be affected by the NSs when both are in contact. In Fig. 3(c), the corresponding SF is shown for the sake of completeness, revealing strong SF enhancements with dipolar character at the LSPR.

There are four results that allow us to state that Au NSs are good candidates as heat sources. Firstly, every single star heats more efficiently than its equivalent sphere, since for all the stars $\tau_E > 1$. Moreover, S_1, S_2, S_3, S_4 are able to heat up from two to seven times more efficiently, and S_5, S_6 more than an order of magnitude. Secondly, τ_E increases when the number and/or the sharpness of the NS tips increases. Sharp (realistic) Au NS with S_4 symmetry yield a temperature enhancement of $\tau_E = 32$. Bear in mind that the fabrication of metallic NSs by chemical shaping of spheroidal nanoparticles in a colloidal suspension [13, 25–28] does not allow full control over the number of tips or the sharpness of the NPs. Therefore it is extremely important that any nanostar in a colloid with $r_{\text{eff}} \gtrsim 40$ nm be a more efficient heater that the equivalent nanosphere, thus making unnecessary the use of any technique to isolate NSs with specific number of tips, dimensions, or tip sharpness. In addition, NSs obtained by chemical techniques usually have a large number of tips; we have shown that this fact improves the heating efficiency of the nanoparticles either. Moreover, it has been shown that a larger number of tips

#155373 - $15.00 USD Received 27 Sep 2011; revised 2 Dec 2011; accepted 6 Dec 2011; published 23 Dec 2011

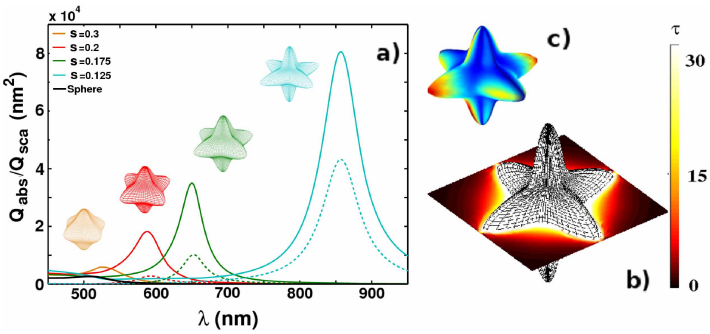

Fig. 3. (a) Absorption Q_{abs} (solid curves) and scattering Q_{sca} (dashed curves) cross sections for S_4 (Au) NSs with constant volume and increasing sharpness for the vertexes, along with those for the equivalent Au nanosphere. (b) Temperature relative factor distribution map near to the sharpest Au nanostar S_4, labeled as $s = 0.125$ in Fig. 3 (cyan), illuminated at its LSPR, $\lambda = 860.2$ nm. (c) Corresponding SF map at the LSPR.

red-shifts the LSPR of the nanostar. The availability of LSPR in the IR reduces the energy of the impinging beam needed to heat NPs up, which makes more unlikely damaging non-cancerous cells. Thirdly, the sharpness of the NS vertexes can be used to tune the ratio Q_{abs}/Q_{sca}. It has been reported [6] that metal NPs with large values of Q_{abs} along with Q_{sca} have applications in photothermal ablation of tumours, with the advantage that the increased near-infrared scattering results also in an enhancement of the optical contrast for optical coherence tomography imaging. Fourthly, note that the reported Q_{abs} are of the same order of that of Au [24]; then $\tau_E^{NS} \gtrsim \tau_E^{dim}$, since $r_{eff}^{NS} < r_{eff}^{dim}$. Thus metallic NSs not only have comparable performance to dimers in SERS, but also in optical heating.

Finally we have to point out that the discussion of the whole article is focused on the parameter τ_E, which is normalized to that of the equivalent sphere, so that the thermal conductivity of the surrounding medium is irrelevant. In practice, to determine absolute values of temperature, water should be considered as the most appropriate surrounding medium.

4. Conclusions

In conclusion, we have described in this work the properties of Au nanostars as thermal heaters based on their large absorption cross sections at the LSPR, and their suitability for cancer thermal therapy. We have shown that their heating properties, resulting from the NS symmetry and geometrical dimensions, are excellent for a variety of optical heating applications; indeed, a $\sim$ 30-fold increase in the steady-state temperature is found for realistic NSs. Additionally, the red-shift induced on the LSPR for increasing number and/or sharpness of NS tips shows that a wide range of frequencies in the visible and near-IR can be covered with various NS shapes. Moreover, the NS tip sharpness rules also the ratio Q_{abs}/Q_{sca}; tuning this ratio, in such a way that Q_{sca} is also large, is a key feature for increasing the optical contrast, thus improving the quality of the optical coherence tomography imaging. Our results confirm that typical Au NSs available with current nanofabrication techniques should no doubt be suitable for photothermal cancer applications.

Acknowledgments

The authors acknowledge support both from the Spain Ministerio de Ciencia e Innovacin through the Consolider-Ingenio project EMET (CSD2008-00066) and NANOPLAS (FIS2009-11264), and from the Comunidad de Madrid (grant MICROSERES P2009/TIC-1476).

#155373 - $15.00 USD Received 27 Sep 2011; revised 2 Dec 2011; accepted 6 Dec 2011; published 23 Dec 2011